Robotica (2014) volume 32, pp. 1383–1397. © Cambridge University Press 2014
doi:10.1017/S0263574714002306

Testing models of cerebellar ataxia via dynamic simulation

David Grow†*, Amy J. Bastian‡
and Allison M. Okamura§

†*Department of Mechanical Engineering, New Mexico Institute of Mining and Technology, Socorro, NM 87801, USA. E-mail: dgrow@nmt.edu*
‡*John Hopkins School of Medicine, Baltimore, MD 21205, USA*
§*Mechanical Engineering Department, Stanford University, Stanford, CA 94305, USA*

(Accepted August 4, 2014. First published online: September 23, 2014)

SUMMARY
Patients with damage to the cerebellum make reaching movements that are uncoordinated or "ataxic." One prevailing hypothesis is that the cerebellum functions as an internal model for planning movements, and that damage to the cerebellum results in movements that do not properly account for arm dynamics. An exoskeleton robot was used to record multi-joint reaching movements. Subsequently, joint-torque trajectories were calculated and a gradient descent algorithm found optimal, patient-specific perturbations to actual limb dynamics predicted to reduce directional reaching errors by an average of 41%, elucidating a promising form of robotic intervention and adding support to the internal model hypothesis.

KEYWORDS: Robotic assistance; Rehabilitation; Cerebellar ataxia.

1. Introduction

1.1. Cerebellar ataxia

Damage to the nervous system often results in altered movement control. The NIH estimates that the neurological disorders strike 50 million Americans each year.[1] In this paper, cerebellar deficits in reaching movements and theoretical ideas about cerebellar function are investigated.

The cerebellum is a region of the brain, directly above the brain stem, known to be essential to generating smooth, accurate reaching movements, but its exact role is not completely understood. Damage to the cerebellum, whether from hereditary disease or stroke, results in ataxia. Ataxia is a lack of coordination of volitional movements and is characterized by the errors in the rate, regularity, and range of movements seen in patients.[2,3] Point-to-point movements made by people with damage to the cerebellum are often composed of an initial movement that under- or overshoots the target (dysmetria), followed by a series of erroneous attempts at correction (intention tremor).[4] Cerebellar patients often use a strategy in which they decompose multi-joint movements into a sequence of single-joint movements, presumably to simplify the effects of movement dynamics. In addition, cerebellar patients have difficulty adapting to changes in environment dynamics.[5–8] There are no proven pharmacological treatments for ataxia.

The study of cerebellar ataxia is of particular interest because there exist specific hypotheses about the nature of the deficit that are related to the dynamics of the body. Investigation of the movements of cerebellar patients may lead to a model of ataxia with sufficient predictive power to inform targeted rehabilitation strategies. Furthermore, the study of the role of the cerebellum is important for understanding motor control in healthy people.

* Corresponding author. E-mail: dgrow@nmt.edu

https://doi.org/10.1017/S0263574714002306 Published online by Cambridge University Press

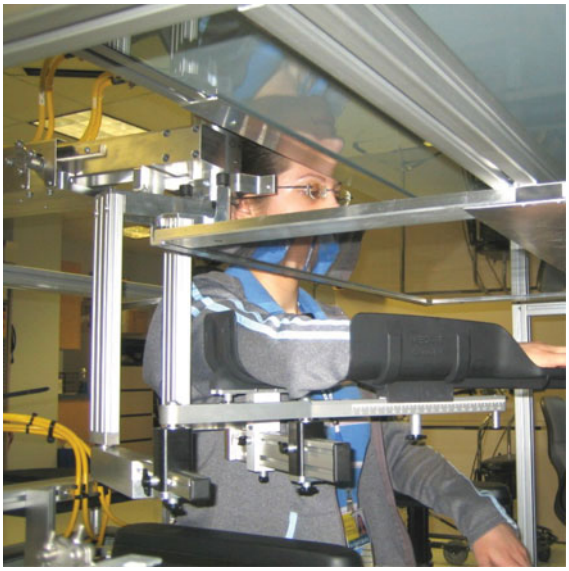


Fig. 1. (Colour online) The KINARM robot used in this study has a two-degree-of-freedom planar exoskeleton for each arm (only right arm shown for clarity).

The feasibility of uncovering cerebellar function and discovering a model of ataxia is bolstered by the availability of high-fidelity robotic exoskeletons. Embedded sensors and actuators permit a means of recording and manipulating mechanical features of movement not possible by human intervention, which, in turn, permits an exploration of the function of the cerebellum and other brain areas[7–10] (Fig. 1). The field of rehabilitation robotics relies on robots both to develop models of the deficit, permitting optimal interventions, and to precisely deliver a prescribed mode of therapy.

1.2. Inverse internal model hypotheses

During movement, various sensory systems, including the vestibular system, vision, and proprioception, provide feedback. However, information from these peripheral sensory sources is not available during early movement. Thus, the brain must act to control movement in an open-loop fashion, based on a belief about the dynamics of the body and environment. If these dynamics have not been learned, or have suddenly changed, the actual movement will not match the intended movement.

It is not known how the cerebellum coordinates reaching movements, or precisely what function is lost when it is damaged. In accordance with the known neural inputs and outputs of the cerebellum, it has been suggested that the role of the cerebellum may be to predict the path of a movement given an efferent copy of the motor commands (forward dynamics)[11,12] or to help predict optimal motor commands given desired movements (inverse dynamics).[13,14] Thus, cerebellar ataxia might result from errors made during these dynamic calculations.

It has been shown that cerebellar patients show disrupted control of limb dynamics in a manner consistent with a dysfunctional internal model.[4,15] For example, cerebellar patients often use a strategy in which they decompose multi-joint movements into a sequence of single-joint movements, presumably to simplify movement dynamics.[4] A variety of specific models of the cerebellum have been proposed that could be used to make quantitative predictions of ataxia.

1.2.1. Cerebellum and velocity-dependent and interaction torques. In particular, studies have shown that people with cerebellar damage have difficulty accounting for Coriolis, centripetal, and interaction torques—even during everyday reaching movements.[4,16,17] Bastian *et al.* demonstrated that cerebellar subjects show deficits in predicting and adjusting for interaction torques occurring at a given joint due to motions of mechanically linked joints. However, performance approaches normal when movements are constrained to a single joint, eliminating the need to predict and compensate for interaction torques.[17] This work suggests that these abnormalities (i.e. ataxia) are due to an inability to predict and compensate for interaction torques that occur during multi-jointed movements, consistent with a dysfunctional internal model.

https://doi.org/10.1017/S0263574714002306 Published online by Cambridge University Press

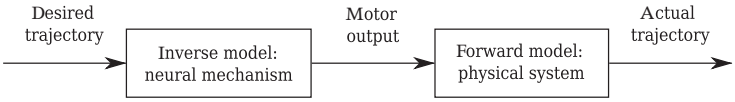


Fig. 2. The modeled process of motor control during early movement. The desired trajectory is specified by the experiment. We assume that a neural mechanism in the cerebellum mirrors the input–output characteristics of the object to be controlled in order to realize the desired trajectory.

1.2.2. Cerebellum and inertia anisotropy. Other studies suggest that ataxia is essentially an inability to account for anisotropic inertial forces.[11,18] Smith developed a robotic system that dynamically canceled some of the inertial effects with the aim of reducing the severity of ataxia.[9] The effect of the inertial compensator on three patients with cerebellar damage was measured using a timed tracing task. One patient who had pure cerebellar ataxia showed a significant improvement in tracing accuracy under inertial compensation, when compared with uncompensated motions.

1.2.3. Other models of cerebellar function. It has also been suggested that true arm dynamics are approximated in a simplified calculation (e.g. characteristic timing pattern of agonist/antagonist).[19] It is not clear how to design an experiment to test a mistiming hypothesis for ataxia with specificity, nor how a mistiming model would translate into an approach for assistance or therapy.

Regardless of how the cerebellum or other brain regions account for dynamics in motion planning, net joint torques and arm motion are precisely related by classical mechanics. Accurate feedforward calculations would need to account for limb dynamics that are nonlinear and anisotropic and potentially depend on a large set of constituent parameters (length, mass, rotational inertia, etc.). While it is unlikely that the cerebellum encodes these dynamics explicitly, model-based interpretations of the cerebellum may well approximate its behavior and are attractive from an analytical perspective.

We use an explicit inverse internal model framework (Fig. 2) to describe early movement. This model assumes that the cerebellum acts as an inverse dynamics calculator. Thus, before feedback is available, ataxia is a manifestation of a misestimation of limb dynamics, constant in time and across direction (i.e. no learning occurs). This means that the model should be able to capture the systematic, but not trial-to-trial, variable nature of movement errors. Within this framework, we test four hypotheses about the nature of ataxia from the literature:

Hypothesis 1: The misestimation is general, not taking any particular form.
Hypothesis 2: The misestimation is a neglect of Coriolis, centripetal, and interaction torques.
Hypothesis 3: The misestimation is a neglect of the arm inertia anisotropy in extrinsic (Cartesian) coordinates.
Hypothesis 4: The misestimation is a neglect of the arm inertia anisotropy in intrinsic (joint-space) coordinates.

For each hypothesis, we searched for a set of errors in the corresponding dynamic parameters that is consistent with the ataxic reaches of people with cerebellar damage.

2. Methods

We tested these hypotheses by collecting reaching data and running dynamic simulations. First, we recorded the movements of control and cerebellar subjects reaching in multiple directions. Using a dynamic model of the human arm and robot, we calculated the net joint torque trajectories for each reaching direction (inverse dynamics). In simulation, we recreated the path given this torque trajectory and any desired dynamic model (forward dynamics). Effectively, we determined the movements that would result if the same torque trajectory were applied to a plant (patient arm) with altered dynamics.

2.1. Exoskeleton robot and human models

In order to precisely specify a desired movement and faithfully record the movement itself, we used the KINARM robot exoskeleton shown in Fig. 1 (BKIN Technologies, Kingston, ON[20]). The KINARM is an adjustable exoskeleton that permits bimanual shoulder and elbow rotation in the horizontal plane. An advantage of the exoskeletal structure is that arm segment length parameters are readily and precisely determined during a calibration procedure after the robot is adjusted to fit

https://doi.org/10.1017/S0263574714002306 Published online by Cambridge University Press

a subject. Motors at the base of a five-bar linkage can generate shoulder and elbow torques of up to 12 N m. Including the effect of a 4:1 gearing, 20,000-count-per-revolution encoders yield a joint angle resolution of $<1/200^{\circ}$. Control of the robot was provided by a real-time computer operating on a 2-kHz clock. The motion control card collects data at 1.129 kHz, which is then filtered, subsampled, and sent to a data acquisition card at 1 kHz. Velocity traces were derived from the position signal using numerical differentiation, improved by $\frac{1}{T}$ interpolation. Acceleration traces were obtained using two 2-g, three-axis accelerometers (Crossbow Technology, Inc., San Jose, CA) incorporated into each arm. For safety, we added foot and hand switches to allow the user to cut power to the robot at any time.

The forward and inverse kinematic equations that relate fingertip positions to shoulder and elbow angles were derived geometrically, using the joint variables and segment lengths defined for the right arm in Fig. 3. The forward kinematic equation for the right arm is

$$\begin{bmatrix} x \\ y \end{bmatrix} = \begin{bmatrix} l_1 c_1 + l_2 c_{12} - l_f s_{12} \\ l_1 s_1 + l_2 s_{12} + l_f c_{12} \end{bmatrix}, \tag{1}$$

where:

$$\begin{aligned} c_1 &= \cos(\theta_1), \\ s_1 &= \sin(\theta_1), \\ c_{12} &= \cos(\theta_1 + \theta_2), \\ s_{12} &= \sin(\theta_1 + \theta_2). \end{aligned}$$

For the left arm, the sign of x is flipped because the angles are defined with mirror symmetry.

The inverse kinematic equations are used to compute shoulder and elbow angles from fingertip position (Fig. 3). The joint angles are given in terms of intermediate variables $\phi_1 \ldots \phi_4$:

$$\begin{bmatrix} \theta_1 \\ \theta_2 \end{bmatrix} = \begin{bmatrix} \phi_1 - \phi_2 \\ \phi_3 - \phi_4 - \theta_1 \end{bmatrix}, \tag{2}$$

where (using arctan2, the four-quadrant inverse tangent):

$$\begin{aligned} \phi_1 &= \arctan2(y, x), \\ \phi_2 &= 2\ \arctan2\left(\sqrt{2\, l_1 l_{0f} - l_1^2 - l_{0f}^2 + l_{1f}^2}, \quad \sqrt{2\, l_1 l_{0f} + l_1^2 + l_{0f}^2 - l_{1f}^2}\right), \\ \phi_3 &= \arctan2(y - l_1 s_1, x - l_1 c_1), \\ \phi_4 &= \arctan2(l_f, l_2), \\ l_{0f} &= \sqrt{x^2 + y^2}, \\ l_{1f} &= \sqrt{l_2^2 + l_f^2}. \end{aligned}$$

The equation of motion of the arm was derived using the Euler–Lagrange equations. The general dynamic equation, assuming that both the human and the robot are applying torque, is

$$\begin{bmatrix} \tau_1 \\ \tau_2 \end{bmatrix} = \begin{bmatrix} a(\theta_2) & b(\theta_2) \\ b(\theta_2) & c \end{bmatrix} \begin{bmatrix} \ddot{\theta}_1 \\ \ddot{\theta}_2 \end{bmatrix} + \begin{bmatrix} 0 & -2d(\theta_2) & -d(\theta_2) \\ d(\theta_2) & 0 & 0 \end{bmatrix} \begin{bmatrix} \dot{\theta}_1^2 \\ \dot{\theta}_1 \dot{\theta}_2 \\ \dot{\theta}_2^2 \end{bmatrix}, \tag{3}$$

https://doi.org/10.1017/S0263574714002306 Published online by Cambridge University Press

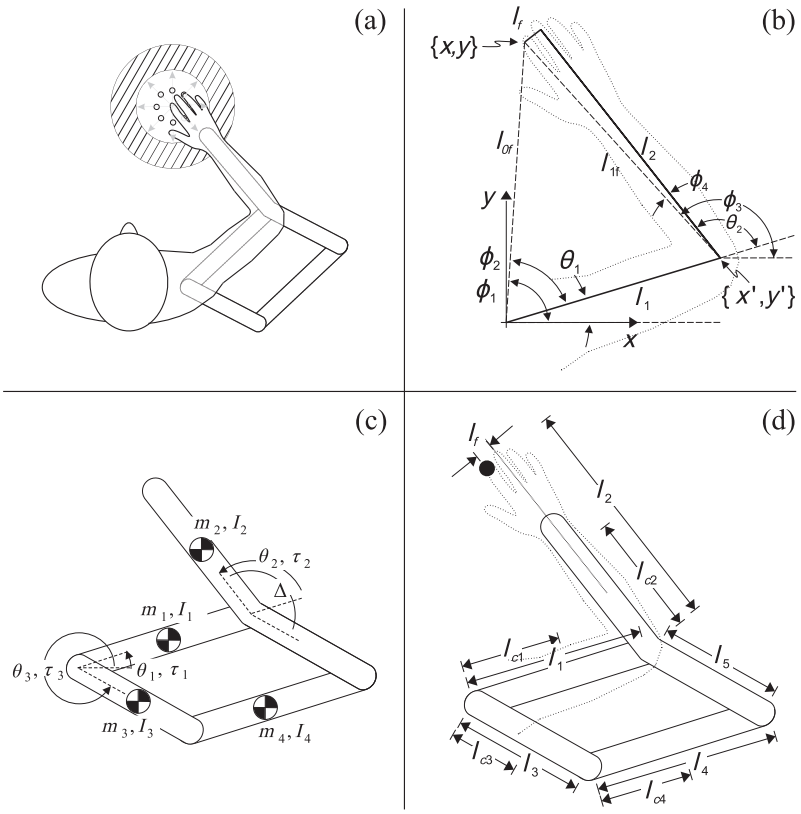


Fig. 3. Kinematic and dynamic variables for the human arm and robot exoskeleton. (a) Arm attached to five-bar linkage allowing shoulder and elbow rotation. In a horizontal reaching task, targets with 1-cm diameter appear 3 cm from start position. Subjects move from the start position, past a target, to a distance of 7 cm, where a virtual wall assists them in stopping (stiffness: 1.5 N/cm, damping: 0.05 N s/cm). (b) Kinematic parameters including upper and lower arm segment lengths and finger offset. (c) & (d) Center of mass parameters for the *combination* of arm and robot.

or

$$\tau = M(\theta)\ddot{\theta} + C(\theta, \dot{\theta}), \tag{4}$$

where:

$$\begin{aligned}
a &= m_1 l_{c_1}^2 + m_2(l_1^2 + 2l_1 l_{c_2}\cos(\theta_2) + l_{c_2}^2) + m_3 l_{c_3}^2 \\
&\quad + m_4(l_3^2 + 2l_3 l_{c_4}\cos(\theta_2 - \Delta) + l_{c_4}^2) + I_1 + I_2 + I_3 + I_4, \\
b &= m_2(l_1 l_{c_2}\cos(\theta_2) + l_{c_2}^2) + m_3 l_{c_3}^2 \\
&\quad + m_4(l_3^2 + l_3 l_{c_4}\cos(\theta_2 - \Delta)) + I_2 + I_3, \\
c &= m_2 l_{c_2}^2 + m_3 l_{c_3}^2 + m_4 l_3^2 + I_2 + I_3, \\
d &= m_2 l_1 l_{c_2}\sin(\theta_2) + m_4 l_3 l_{c_4}\sin(\theta_2 - \Delta), \\
\tau_1 &= \tau_{\text{human shoulder}} + \tau_{\text{robot shoulder}} + \tau_{\text{robot elbow}}, \\
\tau_2 &= \tau_{\text{human elbow}} + \tau_{\text{robot elbow}}, \\
\Delta &= 166^\circ.
\end{aligned}$$

When human torques are set to zero and changes of variables are made, this solution is equivalent to that derived by Scott[20] using D'Alembert's principle.

https://doi.org/10.1017/S0263574714002306 Published online by Cambridge University Press

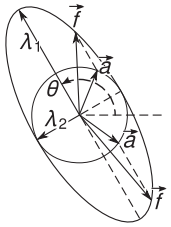


Fig. 4. Force and acceleration vectors are related by the inertia ellipse geometrically (based on ref. [21]). A line drawn along the direction of force until it intersects a circle that circumscribes the inertia ellipse and then continues parallel to the major axis until it intersects the inertia ellipse approximates the resulting acceleration.

Over the small (relative to limb segment lengths) displacements observed during early movement, the dependence of the dynamic parameters on joint configuration (θ_1 and θ_2) is negligible. Thus, we simplify (3) by taking $\{a, b, d\} \equiv (a(\theta), b(\theta), d(\theta))|_{\theta=\theta_0}$:

$$\begin{bmatrix}\tau_1\\ \tau_2\end{bmatrix} = \begin{bmatrix}a & b\\ b & c\end{bmatrix}\begin{bmatrix}\ddot{\theta}_1\\ \ddot{\theta}_2\end{bmatrix} + \begin{bmatrix}0 & -2d & -d\\ d & 0 & 0\end{bmatrix}\begin{bmatrix}\dot{\theta}_1^2\\ \dot{\theta}_1\dot{\theta}_2\\ \dot{\theta}_2^2\end{bmatrix}. \tag{5}$$

This is the form of the dynamic equation used in all simulations. However, this form is still too complex to permit an intuitive understanding of the role the individual dynamic parameters in the force/acceleration relationship. If we further simplify (5) by dropping velocity-dependent terms and transform to extrinsic (Cartesian) coordinates, we obtain a representation described by Dolan *et al.*:[21]

$$\begin{aligned}\begin{bmatrix}F_x\\ F_y\end{bmatrix} &= (J^T)^{-1}\begin{bmatrix}a & b\\ b & c\end{bmatrix}J^{-1}\begin{bmatrix}\ddot{x}\\ \ddot{y}\end{bmatrix}\\ &= \begin{bmatrix}\alpha & \beta\\ \beta & \gamma\end{bmatrix}\begin{bmatrix}\ddot{x}\\ \ddot{y}\end{bmatrix},\end{aligned} \tag{6}$$

where J is the Jacobian and F is the applied force. In this formulation, the mass matrix is interpreted in Cartesian coordinates with the parameters $\{\alpha, \beta, \gamma\}$ encoding an inertia ellipse whose axis lengths and orientation $\{\lambda_1, \lambda_2, \theta\}$ are obtained by eigendecomposition (Fig. 4). The four hypotheses described in Section 1.2 all assert that loss of cerebellar function results in a degraded internal model of limb dynamics. However, each imposes structure on the type of errors that can be considered. In other words, each prescribes constraints to the class of dynamic model that is hypothesized to be used erroneously during the planning of movement. The Dolan approximation permits insight into the constraints imposed by each of the hypotheses we test. The constraint sets corresponding to each hypothesis are enumerated and described in Fig. 5.

2.2. Robot and human dynamic parameter estimation

The creator of the KINARM published equations for calculating its inertial parameters.[20] To validate these calculations, we performed system identification experiments by manually applying force perturbations to the exoskeleton through a Mini40 force/torque sensor (ATI Industrial Automation, Inc., Apex, NC). To identify the parameters of each degree of freedom in the exoskeleton, one joint was perturbed at a time while the other was locked mechanically. The objective function used was obtained by modifying (5) to account for the decoupled dynamics while also including viscous friction (f_{c_i}), Coulomb friction (f_{b_i}), and joint stiffness (k_i) parameters in case they were present to a significant degree:

$$\tau_{\text{robot shoulder}} = a\ddot{\theta}_1 + f_{b_1}\dot{\theta}_1 + f_{c_1}|\dot{\theta}_1| + k_1(\theta_1 - \theta_{1_0}), \tag{7}$$

$$\tau_{\text{robot elbow}} = c\ddot{\theta}_2 + f_{b_2}\dot{\theta}_2 + f_{c_2}|\dot{\theta}_2| + k_2(\theta_2 - \theta_{2_0}). \tag{8}$$

https://doi.org/10.1017/S0263574714002306 Published online by Cambridge University Press

Table I. Sample dynamic parameters identified using ordinary least squares.

Lower-arm parameters (via elbow motion)					
Condition	$I_{\text{predicted}}$	I (kg m^2)	f_c (N m)	b (N m s/rad)	R^2
Baseline	0.0612	0.0605	0.0383	0.0134	0.98
Add 1 mass	+0.104	+0.107	0.0438	0.0240	0.97
Add 2 masses	+0.154	+0.159	0.0326	0.0238	0.97
Upper-arm parameters (via shoulder motion)					
Condition	$I_{\text{predicted}}$	I (kg m^2)	f_c (N m)	b (N m s/rad)	R^2
Baseline	0.103	0.116	0.0301	0.0569	0.95
Add 1 mass	+0.041	+0.038	0.0295	0.0183	0.96
Add 2 masses	+0.106	+0.076	0.0151	0.0142	0.96

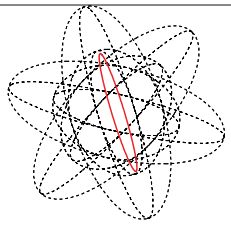
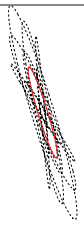
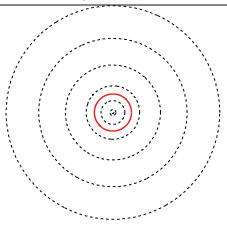
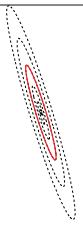
Constraint name	1. No constraints	2. Interaction torque constraints	3. Isotropy$_{\text{ext}}$ constraints	4. Isotropy$_{\text{int}}$ constraints
Parameter constraints	None	$b = 0$, $d = 0$	$\alpha = \gamma$, $\beta = 0$	$a = c$, $b = 0$
Inertia ellipse				
Ellipse DOF	Full (3)	Scale & limited orientation	Scale only	Scale only

Fig. 5. (Colour online) Four classes of error optimization corresponding to our four hypotheses are explained. For each hypothesis, the corresponding dynamic constraints (see (5) and (6)) are shown along with the initial condition to the optimization (solid red) and representative ellipses allowed by the constraints (dashed black). Each optimization is initialized with parameters $\{a, b, c\}$ chosen to keep the area of the inertia ellipse equal to baseline, and the parameter d equals either the baseline value or 0 depending on the constraints. Note that all constraints allow at least two total degrees of freedom (DOF) as Constraint Sets 1, 3, and 4 permit variations in d.

A factor analysis indicated that this addition is not necessary. That is, suitable condition numbers were only obtained once these parameters were eliminated from the objective function before ordinary least squares regression.[22] Robot parameter values vary with arm tray sizes, tray locations, etc. Representative system identification results are shown in Table I. Though robot friction parameters were identified, we did not incorporate them into (3) because their calculated effect on the dynamics of a typical reach is negligible.

The dynamic parameters of the human arm were calculated using predictive tables from Dempster.[23] These tables provide equations for various limb segment inertia parameters given a subject's height and weight, based on cadaver studies.

2.3. Obtaining baseline trajectories for a horizontal reaching task

We recorded baseline movement behavior from one healthy subject and seven cerebellar subjects as they performed a horizontal reaching task (Fig. 3(a)). The subjects showed no signs of sensory loss or extracerebellar damage. The severity of cerebellar impairment was determined using the International Cooperative Ataxia Rating Scale (ICARS).[24] Table II lists cerebellar subjects ordered by the ICARS kinetic functions subscore, which assesses voluntary limb movements. Scores range from 0 (normal) to 52 (severe). Subject diagnosis is based on medical history, family history, and a neurological examination. The cause of ataxia may be focal damage to cerebellar tissue (stroke or trauma), genetic (ADCA, SCA6, and SCA8), or unknown (sporadic).[25] Subjects underwent clinical testing to assess light touch and proprioception of the hand/arm, spasticity, weakness, and extrapyramidal signs. Only

https://doi.org/10.1017/S0263574714002306 Published online by Cambridge University Press

Table II. Subject characteristics and experiment/simulation results.

Subject	Sex	Dom. Hand	Age (yr)	Height (m)	Weight (kg)	Diagnosis	Limb score	RMS baseline error (deg)	RMS simulated error (deg)[b]	Reduction in error (%)
Control	M	R	30	1.80	82	-control-	-control-	1.74	1.71	1.3
Cerebellar 1	M	R	75	1.63	77	stroke	13/52	12.0	7.49	37.5
Cerebellar 2	F	R	52	1.58	51	stroke	15/52	6.13	4.08	33.5
Cerebellar 3	F	R[a]	20	1.68	64	trauma	18/52	10.2	10.2	0.1
Cerebellar 4	F	R	65	1.68	61	sporadic	18/52	6.35	2.65	58.2
Cerebellar 5	M	L	37	1.78	123	SCA8	20/52	14.0	5.27	62.5
Cerebellar 6	M	R	56	1.80	90	SCA6,8	23/52	15.1	5.59	62.9
Cerebellar 7	M	L	57	1.70	96	ADCA	25/52	23.2	14.9	35.9

[a]The non-dominant arm (affected side) was tested.
[b]Result of unconstrained optimization.

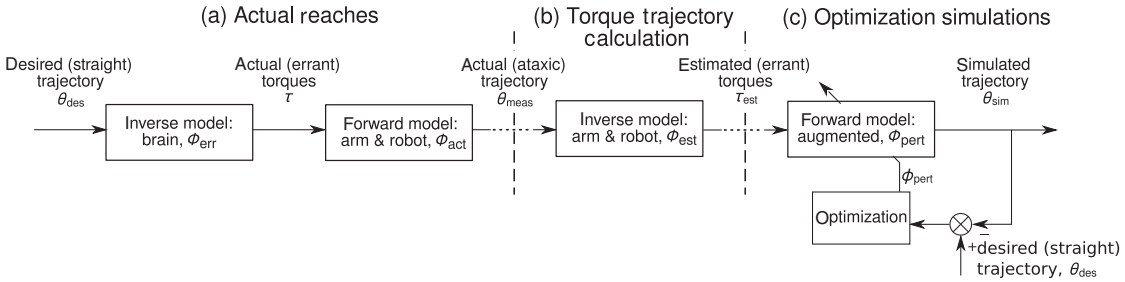


Fig. 6. Experiment and simulation procedure. (a) Cerebellar subjects perform a reaching task in which a desired trajectory is specified visually through display of start, finish, and current finger location. The actual ataxic trajectory is recorded. The intermediate process cannot be observed directly, but is modeled assuming that the actual dynamic parameters of the arm, Φ_{act}, are misrepresented as (Φ_{err}). Motions and forces are represented in joint space because this encoding is more biologically plausible. (b) We calculate the errant torque trajectory, τ, for a given reach using the recorded movement, θ_{meas}, and our estimate of the actual dynamic parameters of the arm, Φ_{est}. (c) The dynamics of the arm are modeled in a computer simulation. A set of dynamic parameters, Φ_{pert}, are optimized to reduce movement error, θ_{sim}, relative to the reference trajectory, θ_{des}, when the subject's torque trajectory is applied. Torque and joint trajectories are $n \times 2$ matrices, describing both elbow and shoulder joints over some time interval.

the subject who had a traumatic head injury showed the addition of mild spasticity and mild weakness. Other subjects were unimpaired in all of these domains. All subjects gave informed consent to the protocols approved by the Johns Hopkins Medical Institutions Review Board, study NA_00015034.

At the beginning of each trial, the subject moved to a center position (shoulder at 35°, elbow at 90°). After a slight delay, one of eight radial targets appeared. The choice of a ballistic, punch-through task with near targets, rather than a point-to-point task with distant targets, was made to ensure that the trajectory during early movement was clearly specified. Subjects were encouraged to pass through the target within a 350–500 m s window and then continue moving until a force field near the workspace boundary brought them to a stop. The robot otherwise applied no force to the user during the task. Movement duration feedback was given to the subjects in the form of color coding: the target turned blue if passed late, red if early, or green if on time. During the task, targets appeared in pseudo-random order. Trials were divided into three blocks: a practice block and two analyzed blocks. Each block included 10 reaches to each of the eight targets. All trials in the last two blocks were analyzed, whether or not the timing criteria were met.

2.4. Simulating the effects of altered dynamics

The four hypotheses described in Section 1.2 all assume the cerebellum functions as an internal model for planning movements and that, in part, damage to the cerebellum results in a biased (inaccurate) model. This bias is identified for cerebellar subjects, individually, using the procedure depicted in Fig. 6.

https://doi.org/10.1017/S0263574714002306 Published online by Cambridge University Press

By this point, two steps have been performed. First, the movements of subjects ($\vec{\theta}_{\text{meas}}$) have been recorded as they attempt to follow straight paths to the goal ($\vec{\theta}_{\text{des}}$, Fig 6(a)). Trial data were clipped to a 300-m s window centered at the point in time at which hand speed exceeded 10% of the maximum for that reach. This early movement window captures open-loop behavior and extends long enough for the dynamics to have a significant effect on the reach. Second, we calculated the net joint torques exerted during the movement window by each subject (inverse dynamics) using this kinematic data, the subject's actual dynamic parameters ($\vec{\phi}_{\text{est}}$), and the equation of motion (5) (Fig. 6(b)). Finally, the 10 joint angle and torque trajectories were averaged for each target.

These torque trajectories were then used in simulations to compute (forward dynamics) hand paths given different dynamic parameters ($\vec{\phi}_{\text{pert}}$, Fig. 6(c)). Because the equation of motion is nonlinear, the forward dynamics were computed numerically using Euler integration after re-expressing (4) as

$$\ddot{\theta} = M^{-1}(\tau - C(\dot{\theta})). \tag{9}$$

The algorithms used to compute the inverse and forward dynamics were verified by sequentially computing the inverse and forward dynamics using estimated dynamic parameters and recorded reaches. Representative successful replication of the original hand paths is shown in Fig. 7(c)).

We then searched for a perturbation, or modification of the parameters in (5) or (6), that optimally reduced reaching errors within the constraints dictated by each hypothesis (Figs. 5 and 6(c)). An optimal altered dynamic environment cannot be computed directly because the forward dynamic equation does not have an analytic solution. Thus, we searched for an optimal environment through a pseudo-gradient descent over the free parameters permitted by each of the four constraint sets. We first computed the average torque trajectory for each of the eight targets, and for each subject. At each step in the search, we took these torque trajectories and applied them to a set of perturbed plants—the set being derived by taking the current plant and perturbing each of its parameters, individually and pairwise, by a given magnitude. The resulting hand paths were then simulated for each plant. The perturbation that produced the straightest paths from the start position to the targets (without over- or under-shoot) was stored and fed into the next iteration. The magnitude of the perturbations began at 100 times the corresponding parameter's initial value. The optimization algorithm iterated until an error plateau was reached. The perturbation magnitudes were then halved and the process continued. The optimization ended when the step size was reduced to 0.1% of the parameters' original magnitude and another error plateau was reached. This search was repeated for each of the four constraint sets.

3. Results

3.1. Baseline movement data

The baseline trajectories for control and cerebellar reaches were analyzed. As expected, control reaches are nearly straight and directed towards the targets. Cerebellar reaches, however, show errors in movement direction and increased variability. Examples of reach data are shown in Fig. 7.

Inertia dominates the dynamics of all recorded reaches. Acceleration-dependent terms account for an average of 98.5% of joint torques (integrating over early movement using (5)). It follows from this insensitivity to the parameter d that the Dolan approximation faithfully approximates arm dynamics during early movement.

3.2. Validating the optimization scheme using control data

In order to validate the optimization algorithm, the control data was analyzed first. The unconstrained optimization algorithm, as per Hypothesis 1, was able to find a change in dynamics that slightly improved the small errors, though the improvement is not statistically significant (1.74°–1.71° root-mean-squared (RMS) error, $p = 0.53$ (paired t-test)). The predicted optimal dynamic parameters were between those of the arm alone and those of the arm and robot combined. Thus, the optimization found a solution that removed part of the added inertia of the robot. The original and optimized reach directions, angular errors before and after optimization, and inertia ellipses before and after optimization are shown in the first rows of Fig. 8 and Table III. Implementation of Constraint Sets 2, 3,

https://doi.org/10.1017/S0263574714002306 Published online by Cambridge University Press

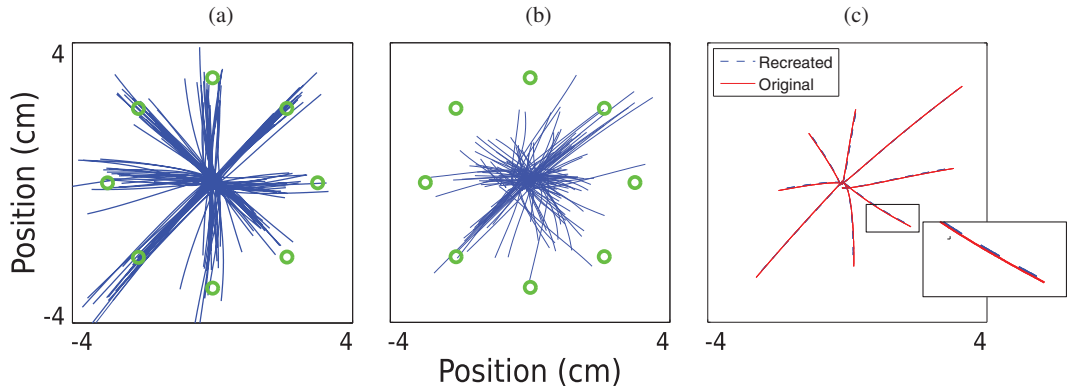


Fig. 7. (Colour online) Example trajectories of the control (a) and Cerebellar 5 (b) subjects. Each subject makes 20 reaches passing through each of eight targets (small circles). The data is clipped to include only the first 300 m s of the reach. (c) Averaged hand paths of Cerebellar 5, the derived equation of motion, and estimated dynamic parameters are used to verify the numerical methods used, by checking that the inverse and forward dynamic calculations are reversible.

and 4 (no interaction torque, inertia isotropy in extrinsic coordinates, and inertia isotropy in intrinsic coordinates, respectively) all resulted in greatly degraded performance, even after optimization.

3.3. Optimization results for cerebellar patients

As with the control subject, the unconstrained optimization found a change in dynamics that improved the direction and extent of reaches of cerebellar patients, whereas implementation of the constraints imposed by Constraint Sets 2–4 (no interaction torque, inertia isotropy in extrinsic coordinates, and inertia isotropy in intrinsic coordinates, respectively) resulted in degraded performance, even after optimization. The optimizations converged in 38, 24, 36, and 32 steps, on average, for Constraint Sets 1, 2, 3, and 4, respectively.

We then determined whether each of these optimal perturbations resulted in a reduction in reaching errors that was statistically significant using a one-way repeated measures ANOVA. Due to violations in the sphericity assumption, a box adjustment was made to the F statistic. Thereafter, multiple comparison of groups were made using dependent t-tests for paired samples.

The constraint sets resulted in outcomes that are statistically different from each other ($F(4,24) = 68.32, p < 0.001, \hat{\epsilon} = 0.39, n = 7$). Under Constraint Set 1 (any perturbation to $\{a, b, c, d\}$ allowed), the optimization found altered dynamics for the cerebellar subjects that produced a statistically significant improvement (mean 41% or -5.3° RMS, $p = 0.009$), see Fig. 8, column (a) and Fig. 9. Constraint Set 2 (no interaction torque) added 18.5° RMS error ($p < 0.001$). Constraint Sets 3 and 4 (enforcing inertia isotropy in extrinsic coordinates and intrinsic coordinates, respectively) added 10.0° RMS and 25.3° RMS error, respectively ($p = 0.01$, $p < 0.001$). Though Constraint Sets 2 and 4 are similar ($b = 0$ in both cases), the difference in performance between them is statistically significant ($p = 0.018$).

Use of RMS angular error as the performance metric results in the optimization giving preference to a perturbation in dynamics that significantly reduces errors in one or more directions even if it comes at the expense of slightly degraded performance in others. In fact, the optimizations under Constraint Set 1 were not always able to find a perturbation that uniformly reduced angular errors for all directions (Fig. 8, column (b)). The choice of another metric could result in different optimal perturbations. For instance, if there is reason to prefer certain directions, a non-uniform weighting could be employed.

4. Discussion

4.1. Validating optimization scheme using control data

The outcome of optimization for the control subject under Constraint Set 1 (any perturbation of $\{a, b, c, d\}$ allowed) is of interest because we found that the optimal inertia ellipse is intermediate to

https://doi.org/10.1017/S0263574714002306 Published online by Cambridge University Press

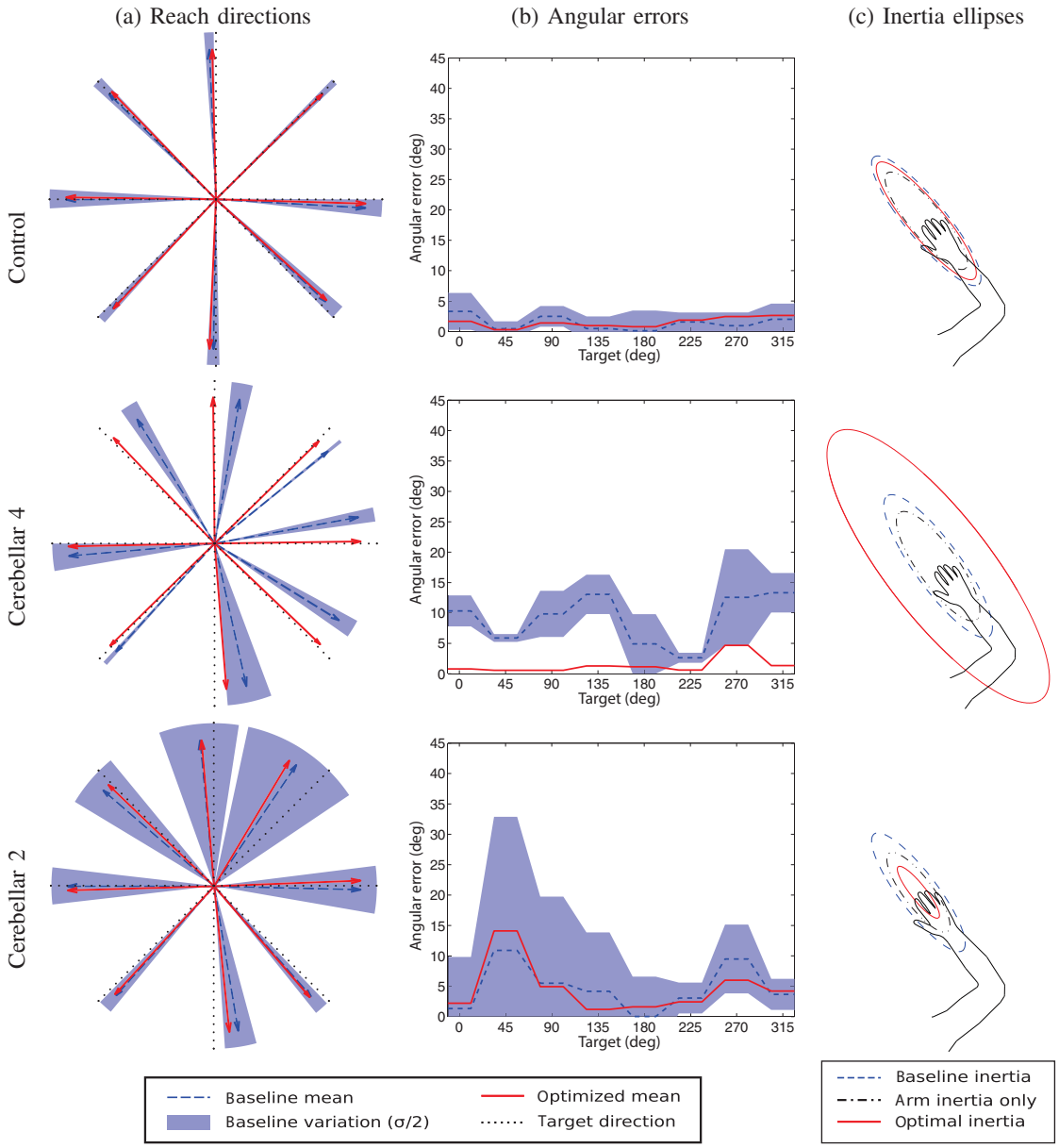


Fig. 8. (Colour online) Optimization results (unconstrained) shown for a control subject and two cerebellar subjects. The cerebellar subjects were chosen to represent good (Cerebellar 4) and poor (Cerebellar 2) outcomes of optimization. (a) Reach direction mean and variation ($\sigma/2$) are calculated from clipped movement data (left) and simulated optimal reaches (right). (b) Angular errors are quantified for each of the eight directions—both absolute mean and variation ($\sigma/2$). The optimization algorithm seeks to minimize RMS angular error, which is different from the metric shown here. (c) Inertia ellipses of the human arm alone, with the robot, and predicted optimum.

the ellipse of the subject's arm alone and that of the combination of arm and robot (Table III, row 1 and Fig. 8, column (b)). This finding is intuitive and suggests that the control subject did not fully adapt to the dynamics of the robot.

4.2. Optimization results

Hypothesis 1 (dynamic parameter error: general case)
This hypothesis permits an unconstrained optimization over four dynamic parameters and resulted in improved average simulated reaching performance for all cerebellar subjects. The gradient descent

https://doi.org/10.1017/S0263574714002306 Published online by Cambridge University Press

Table III. Summary of the optimization results obtained under each of the four constraint sets. The predicted optimal dynamics are described in terms of an inertia ellipse with axis lengths λ_1, λ_2, and orientation θ.

				Constraint sets											
	Baseline			**1. General**			**2. Interaction**			**3. Isotropy$_{ext}$**			**Isotropy$_{int}$**		
Subject	λ_1	λ_2	θ°	λ_1	λ_2	θ°	λ_1	λ_2	θ°	λ_1	λ_2	θ°	λ_1	λ_2	θ°
Control	4.3	1.0	130	3.7	0.89	130	14	1.0	120	50	50	n/a	370	37	107
1	4.2	0.90	130	2.1	0.69	131	7.6	0.62	117	7.3	7.3	n/a	2.8	0.24	110
2	3.2	0.76	127	1.4	0.33	127	8.2	0.54	120	0.14	0.14	n/a	28	3.0	103
3	3.8	0.94	131	3.7	0.92	131	3.4	0.34	116	0.087	0.087	n/a	2.0	0.20	108
4	3.5	0.82	126	5.2	1.5	126	38	2.4	119	0.19	0.19	n/a	38	3.6	104
5	5.8	1.4	126	3.9	1.1	131	368	6.9	124	9.9	9.9	n/a	57	5.1	105
6	4.8	1.2	132	0.34	0.14	134	12	1.1	114	4.5	4.5	n/a	27	2.4	111
7	4.8	1.2	129	5.9	1.5	126	0.29	0.027	117	.92	.92	n/a	3.5	0.37	105

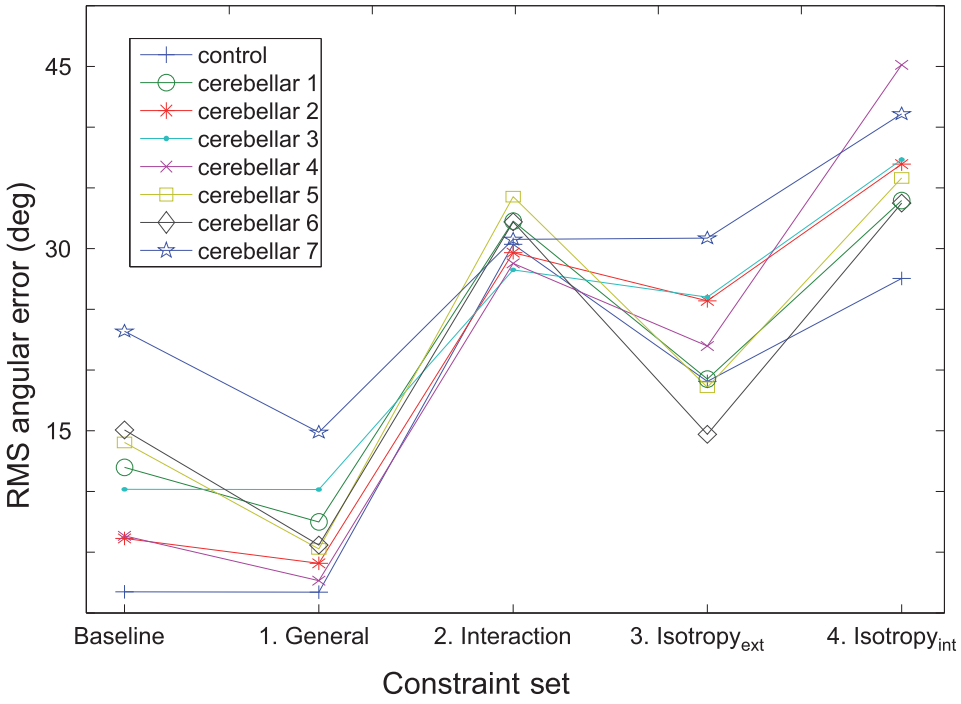


Fig. 9. (Colour online) Baseline errors and residual errors after optimization under four constraint sets are shown for each subject (means: {11.1, 6.5, 30.8, 22.0, 36.4}, standard errors: {2.3, 1.5, 0.7, 1.8, 1.84}). The Constraint Set 1 improves upon baseline error whereas enforcing the constraints of the other constraint sets results in greater than baseline error.

algorithm did converge in all cases. The optimization found inertia ellipses that are substantially different from either those of the subjects' bare arms or those of the arm/robot combinations. For some subjects, the deficit appears to be an underestimation of inertia and for others an overestimation (Table III).

The inability of the optimization under Constraint Set 1 to fully remove reaching error indicates that the model does not fully capture ataxic behavior. Certainly, this type of model cannot predict the higher variability observed in ataxic patients—only systematic biases. It should also be noted that there is no guarantee that the optimization algorithm found the global optimum. Furthermore, it is possible that patients may employ a movement strategy other than the straight-line path assumed by the model. For example, it has been observed that cerebellar subjects tend to segment multi-degree-of-freedom movements into a series of one-degree-of-freedom movements.[17] By design, this particular strategy cannot be used in this experiment because of the tight time constraint used. Despite these

https://doi.org/10.1017/S0263574714002306 Published online by Cambridge University Press

limitations, the model is able to prescribe a dynamics perturbation that reduces reaching error to a substantial degree, even while simultaneously considering its effects in eight directions.

Finally, it appears that subjects with more focal damage were predicted to benefit more from reaching in an augmented-dynamics environment (i.e. consistent with the inverse internal model hypothesis) than subjects whose damage was less specific (e.g. Cerebellar 2 with cerebellar trauma).

Hypotheses 2–4 (specifically neglecting velocity-dependent terms, interaction torques, or inertia anisotropy)

Enforcing the constraints that correspond to Hypotheses 2–4 resulted in simulated reaching performance that was degraded compared to the original reaches. That is, when the optimization algorithm was only allowed to consider diagonal mass matrices (Hypothesis 2) or mass matrices that correspond to isotropic inertia ellipses (Hypotheses 3 and 4), it was unable to find any solution that improved performance. In fact, all resulted in worse-than-baseline performance. This result suggests that, even if the cerebellum acts as an inverse internal model, these subjects do not simply neglect interaction, Coriolis, or centripetal torques or the anisotropic nature of arm inertia during dynamic motion planning.

Upon closer examination, we can see that Constraint Sets 2 and 4 result in similar constraints, and therefore, they prescribe similar parameter subspaces for consideration during optimization. Both set the off-diagonal mass term to zero ($b = 0$). The difference is that Constraint Set 2 allows the diagonal terms $\{a, c\}$ to vary freely, while Constraint Set 4 only allows them to co-vary as equal. The fact that Constraint Set 2 set $d = 0$ and Constraint Set 4 allows it to vary is of little consequence because the velocity-dependent terms have little impact during early movement. It is no great surprise then, that we find no statistical difference in the optimization outcomes under Constraint Sets 2 and 4.

5. Conclusions and Future Work

We tested four hypotheses about the role of the cerebellum in movement control using recorded movements and dynamic simulation. Constraint Set 1 (any perturbation to $\{a, b, c, d\}$ allowed), as dictated by Hypothesis 1, yielded simulated improvements in reaching performance. This is consistent with the idea that the cerebellum functions as an internal model for planning movements, and that damage to the cerebellum results in movements that do not properly account for arm dynamics in a systematic way. It is therefore possible that with appropriate robotic intervention in place, cerebellar patients' movement control might improve. However, the simulations were not able to find any perturbation to arm dynamics that were predicted to fully remove movement errors, indicating that our model does not fully describe the role of the cerebellum in movement control. For larger-scale movements that involve lower-magnitude accelerations, including limb damping and stiffness during optimization might allow for improved predictive power. One of the challenges in doing so would that, unlike inertial parameters, damping and stiffness are not deterministically related to arm configuration. Finding that simulations predict degraded performance under Constraint Sets 2–4 suggests that, even after cerebellar degeneration, the human motor system is able to account, at least partially, for limb inertia anisotropy and interaction, Coriolis, and centripetal torques.

We think that an exoskeleton robot could be used actively to change the effective arm dynamics in accordance with these simulations. More specifically, we expect that augmenting the dynamics of a subject's arm to match an errant inverse model would result in control-like reaching behavior. This would be especially useful because correcting faulty cerebellar patient movements through motor learning has not been effective.[5–8] Our results inspire the design of new rehabilitation strategies for patients with cerebellar damage using patient-specific augmentations to arm dynamics. Such an approach is predicted to generally improve reaching performance without requiring a priori knowledge of the the patients' intended direction of movement.

We recently used the exoskeleton to apply the optimal augmentation in dynamics to cerebellar patients.[26] As part of that work, we developed control methods that provide high-fidelity inertia compensation while maintaining safety and controller stability. Preliminary results indicate that this approach may improve the reaching of some cerebellar patients and not others. Dynamic compensation appears to be more effective for single-joint movements[27] than the planar movements studied here.

https://doi.org/10.1017/S0263574714002306 Published online by Cambridge University Press

This is underscored by force control results showing that cerebellar patients can control force in a single degree of freedom more effectively than in two degrees of freedom.[28]

Acknowledgments

The authors gratefully acknowledge Dr. Steven Charles for his contributions toward the formation of the hypotheses and Dr. Nasir Bhanpuri for his assistance in designing the experiment task protocol and testing subjects. This research was supported in part by Johns Hopkins University, Kennedy Krieger Institute, and National Institutes of Health grants F31 NS061613, R21 NS061189, and R01 HD040289.

References

1. National Institute of Neurological Disorders and Stroke. NINDS Overview. Available at: `http://www.ninds.nih.gov/about_ninds/ninds_overview.htm`. Last accessed: March 31, 2011.
2. R. D. Adams and M. Victor, *The Cerebellum. Principles of Neurology* (McGraw-Hill, New York, 1993).
3. C. Ghez and W. T. Thach, "The Cerebellum," **In**: *Principles of Neural Science* (E. R. Kandel, J. H. Schwartz and T. M. Jessell, eds.) (McGraw-Hill, 2000) pp. 832–852.
4. A. J. Bastian, T. A. Martin, J. G. Keating and W. T. Thach, "Cerebellar ataxia: abnormal control of interaction torques across multiple joints," *J. Neurophysiol.* **76**, 492–509 (1996).
5. G. M. Earhart, W. A. Fletcher, F. B. Horak, E. W. Block, K. D. Weber, O. Suchowersky and J. G. Melvill, "Does the cerebellum play a role in podokinetic adaptation?" *Exp. Brain Res.* **146**(4), 538–542 (2002).
6. T. A. Martin, J. G. Keating, H. P. Goodkin, A. J. Bastian and W. T. Thach, "Throwing while looking through prisms: I. Focal olivocerebellar lesions impair adaptation," *Brain* **119** 1183–1198 (1996).
7. M. Maschke, C. M. Gomez, T. J. Ebner and J. Konczak, "Hereditary cerebellar ataxia progressively impairs force adaptation during goal-directed arm movements," *J. Neurophysiol.* **91**(1), 230–238 (2004).
8. M. A. Smith and R. Shadmehr, "Intact ability to learn internal models of arm dynamics in Huntington's disease but not cerebellar degeneration," *J. Neurophysiol.* **93**(5), 2809–2821 (2005).
9. E. D. Smith, Robotic Compensation of Cerebellar Ataxia *Master's Thesis* (Cambridge, MA: Department of Mechanical Engineering and Department of Electrical Engineering and Computer Science, Massachusetts Institute of Technology, September 2004).
10. H. F. M. Van der Loos, "VA/Stanford rehabilitation robotics research and development program: lessons learned in the application of robotics technology to the field of rehabilitation," *IEEE Trans. Rehabil. Eng.* **3**(1), 46–55 (1995).
11. N. Schweighofer, M. A. Arbib and M. Kawato, "Role of the cerebellum in reaching movements in humans: I. distributed inverse dynamics control," *Eur. J. Neurosci.* **10**(1), 86–94 (1998).
12. D. M. Wolpert and M. Kawato, "Multiple paired forward and inverse models for motor control," *Neural Netw.* **11** 1317–1329 (1998).
13. R. C. Miall, D. J. Weir, D. M. Wolpert and J. F. Stein, "Is the cerebellum a Smith predictor?" *J. Motor Behav.* **25** 203–216 (1993).
14. M. Kawato, "Learning Internal Models of the Motor Apparatus," **In**: *The Acquisition of Motor Behavior in Vertebrates* (Bradford Books, Cambridge, 1996) p. 409.
15. H. Topka, J. Konczak, K. Schneider, A. Boose and J. Dichgans, "Multi-joint arm movements in cerebellar ataxia: Abnormal control of movement dynamics," *Exp. Brain Res.* **119**(4), 493–503 (1998).
16. P. Pigeon, S. B. Bortolami, P. DiZio and J. R. Lackner, "Coordinated turn-and-reach movements. I. Anticipatory compensation for self-generated coriolis and interaction torques," *J. Neurophysiol.* **89**(1), 276–289 (2003).
17. A. J. Bastian, K. M. Zackowki and W. T. Thach, "Cerebellar ataxia: torque deficiency or torque mismatch between joints?" *J. Neurophysiol.* **83**(5), 3019–3030 (2000).
18. S. Massaquoi and M. Hallett, "Kinematics of initiating a two-joint arm movement in patients with cerebellar ataxia," *Can. J. Neurolog. Sci.* **23**(1), 3–14 (1996).
19. H. Gomi and M. Kawato, "Human arm stiffness and equilibrium-point trajectory during multi-joint movement," *Biol. Cybern.* **76**(3), 163–171 (1997).
20. S. H. Scott, "Apparatus for measuring and perturbing shoulder and elbow joint positions and torques during reaching," *J. Neurosci. Methods* **89** 119–127 (1999).
21. J. M. Dolan, M. B. Friedman and M. L. Nagurka, "Dynamic and loaded impedance components in the maintenance of human arm posture," *IEEE Trans. Syst. Man Cybern.* **23**(3), 698–709 (1993).
22. J. Hollerbach, W. Khalil and M. Gautier, Chapter 14: Model Identification," **In**: *Springer Handbook of Robotics* (B. Sciliano and O. Khatib, eds.) (Springer, 2008) pp. 321–342.
23. L. Dempster, *Patterns of Human Motion* (Prentice Hall, Inc., Englewood Cliffs, New Jersey, 1971).
24. P. Trouillas, T. Takayanagi, M. Hallett, R. D. Currier, S. H. Subramony, K. Wessel, A. Bryer, H. C. Diener, S. Massaquoi, C. M. Gomez, *et al.*, "International cooperative ataxia rating scale for pharmacological assessment of the cerebellar syndrome," *J. Neurolog. Sci.* **145**(2), 205–211 (1997).

https://doi.org/10.1017/S0263574714002306 Published online by Cambridge University Press

25. Neuromuscular Disease Center. Ataxias: General Classification. Available at: `http://neuromuscular.wustl.edu/ataxia/aindex.html`. Last accessed: March 31, 2011.
26. D. Grow, A. J. Bastian and A. M. Okamura, "Robotic Assistance for Cerebellar Reaching," **In**: *Neuro-Robotics: From Brain Machine Interfaces to Rehabilitation Robotics* (P. Artemiadis, ed.), vol. 2 (Springer, 2014) pp. 317–343.
27. N. H. Bhanpuri, A. M. Okamura and A. J. Bastian, "Predicting and correcting ataxia using a model of cerebellar function," *Brain* **137** 1931–1944 (2014).
28. S. K. Charles, A. M. Okamura and A. J. Bastian, "Does a basic deficit in force control underlie cerebellar ataxia?" *J. Neurophysiol.* **109**(4), 1107–1116 (2013).

https://doi.org/10.1017/S0263574714002306 Published online by Cambridge University Press